NASA Technical Paper 1530

Traction Drive Performance Prediction for the Johnson and Tevaarwerk Traction Model

Joseph L. Tevaarwerk

OCTOBER 1979

NASA

NASA Technical Paper 1530

Traction Drive Performance Prediction for the Johnson and Tevaarwerk Traction Model

Joseph L. Tevaarwerk
Lewis Research Center
Cleveland, Ohio

National Aeronautics
and Space Administration

**Scientific and Technical
Information Branch**

1979

SUMMARY

The recently developed Johnson and Tevaarwerk fluid rheology model was used to investigate the traction behavior for typical traction drive contacts. Fluid shear modulus and limiting fluid shear strength were allowed to vary over the contact area in accordance with observed traction behavior. The influence of aspect ratio of the contact and the invariably present spin was investigated. Graphical solutions of the analysis are provided which allow for the design optimization of traction drives. Comparisons were made with the commonly used rigid-plastic analysis of Wernitz.

The influence of low spin values on traction was found to be negligible; therefore, the simple slip analysis with the elastic-plastic model is sufficient. At moderate values of spin the complete spin analysis with the elastic-plastic model is needed to give accurate traction predictions. At sufficiently high spin the Johnson and Tevaarwerk model may be simplified to the rigid-plastic model, and the elastic effects in the fluid may be neglected. Contacts with a low aspect ratio predict a superior performance in that they show less slip for the same degree of traction. Sideways forces due to the spin on the contact can be substantial and may reach 75 percent of the transmitted traction force. Also the effect due to spin is always deleterious to the traction efficiency.

INTRODUCTION

Typically the power transmission in continuously variable speed traction drives occurs in a small, elastically deformed region on the two elements. Due to the rolling motion and in the presence of a fluid, a thin layer of lubricant is drawn into this contact area, thus separating the two bodies.

Relative velocities between the two bodies in contact shears the lubricant. Its resistance to shear permits a transmission of force between the two bodies. The amount of force that can be transmitted for a given amount of slip has been the subject of many past and present investigations, many of them resulting in fluid models (refs. 1 to 5).

The fluid in the gap is subjected to very high pressure gradients and pressures for very short times. The common behavior to high pressures is an increase in the viscous shear resistance of the lubricant (refs. 6 and 7), however, due to the extremely short duration of the pressure, the situation is not at all clearly understood. This is because there are no simple experiments that will directly measure the shear properties

of the lubricants. It is known, however, that there are definite time delays in the response of these lubricant properties to sudden pressure changes (ref. 8), and it is thought that the lubricant behaves in a more elastic fashion at low deformation rates (ref. 5).

Due to the uncertainties in the shear response of the fluid, the past design techniques for analyzing traction drive contacts were based upon the rigid-plastic concept as used by Wernitz (ref. 9) and Magi (ref. 10). More recently a refined traction model was proposed and experimentally validated by Johnson and Tevaarwerk (ref. 5) which considers the lubricant behavior to be viscoelastic reducing to an elastic-plastic model at high pressures and shear strains.

The objective of this investigation is to (1) examine the traction behavior of a lubricant for a typical traction drive contact using the Johnson and Tevaarwerk model; (2) generate design charts for traction drive contacts using this model; (3) make a comparison between this new model and the Wernitz-Magi approach; and (4) establish design criteria for the application of either of these models.

SYMBOLS

A	contact area, m^2
a, b	Hertzian contact ellipse parameters; a is the semiaxis in the rolling direction; b is the semiaxis perpendicular to the rolling direction, m
e	speed pole location, m
$\dot{e}_{ij}$	rate of strain tensor, sec^{-1}
F_x, F_y	traction force in x- and y-direction, respectively, N
$F(\tau_e)$	dissipative strain rate function, sec^{-1}
$\overline{F}(Z_e)$	dimensionless strain rate function
G	elastic shear modulus, N/m^2
$\overline{G}$	average elastic shear modulus over contact area, N/m^2
G_c	compliance corrected shear modulus, N/m^2
G_s	elastic shear modulus of disk material, N/m^2
h	film thickness, m
J_1	dimensionless slip in rolling direction
J_3	dimensionless spin
J_4	dimensionless traction in rolling direction

J_5	dimensionless traction perpendicular to rolling direction
J_6	dimensionless spin torque
J_7	dimensionless power loss
k	aspect ratio of Hertzian contact, b/a, dimensionless
m	initial slope of experimental traction curves, dimensionless
m'	initial slope of traction curve for dry rolling bodies, dimensionless
N	normal force on contact, N
P	Hertzian pressure in contact, N/m^2
P_o	maximum Hertzian pressure in contact, N/m^2
T	spin torque on contact, N-m/rad
q	aspect ratio dependent constant, dimensionless
$U^{\pm}$	velocities in x-direction on upper and lower body, m/sec
ΔU	rolling velocity difference (slip), m/sec
$V^{\pm}$	velocities in y-direction on upper and lower body, m/sec
ΔV	velocity difference in y-direction, m/sec
ΔX	dimensionless spin pole offset
X, Y	dimensionless Cartesian coordinates
x, y, z	Cartesian coordinates, m
Z	dimensionless stress
δ_x	spin pole offset, m
ε	dimensionless speed pole location
μ	maximum traction coefficient from experimental traction curve, dimensionless
τ	shear stress, N/m^2
τ_c	reference stress for hyperbolic sinh, N/m^2
τ_o	limiting shear strength of fluid, N/m^2
$\bar{\tau}_o$	average limiting shear strength of fluid over contact area, N/m^2
φ	equivalent strain rate parameter
ω	angular velocity difference between contacting bodies normal to contact area, rad/sec

Subscripts:

e	equivalent
ij	tensor coordinates
x, y, z	Cartesian coordinates

THEORETICAL ANALYSIS

Typically the power transmission in variable speed traction drives occurs in highly stressed contact areas that operate in the elastohydrodynamic lubrication (EHL) regime. The traction characteristics of these drives therefore depend to a large extent on the fluid and material properties at the EHL conditions that prevail. At these conditions of pressure ($\simeq 10^9$ Pa), transit time, (10^{-3} sec), and temperature ($30^\circ \rightarrow 150^\circ$ C), Johnson and Tevaarwerk, in reference 5, found that the shear behavior of the lubricants examined was best described by the following constitutive equation:

$$\frac{d(\tau_{ij}/G)}{dt} + \frac{\tau_{ij}}{\tau_e} F(\tau_e) = 2\dot{e}_{ij} \tag{1}$$

where

τ_{ij}	stress tensor
$\dot{e}_{ij}$	rate of strain tensor
τ_e	equivalent stress, $\sqrt{(\tau_{ij} \cdot \tau_{ij})/2}$
$F(\tau_e)$	nonlinear viscous function to be specified later
G	elastic shear modulus of fluid

Equation (1) was formulated by the simple addition of elastic and viscous compliances to account for the total compliance of the fluid film. Its correctness in formulation was extensively tested and verified in reference 11 using a point-contact-type disk machine that permits the study of traction under both slip, spin, and slip and spin.

To obtain the tractive capacity for a typical traction drive contact, equation (1) has to be solved as a series of coupled differential equations with the proper use of the geometric boundary conditions and the applied rate of strain tensor.

A typical Hertzian contact as it occurs in many forms of traction drives is shown in figure 1 together with the nomenclature that is commonly used. For this simple geometry equation (1) reduces to the following:

$$\left.\begin{aligned} \frac{d(\tau_x/G)}{dt} + \frac{\tau_x}{\tau_e} F(\tau_e) &= 2\dot{e}_x \\ \frac{d(\tau_y/G)}{dt} + \frac{\tau_y}{\tau_e} F(\tau_e) &= 2\dot{e}_y \end{aligned}\right\} \qquad (2)$$

and

$$\tau_e = \sqrt{\tau_x^2 + \tau_y^2}$$

The system of shear stresses acting on the surface gives rise to tractive forces F_y and F_x.

Figure 2 shows the side view of the contact; the following assumptions have been made:

(1) Film thickness h is constant over the contact area.

(2) Pressure distribution is Hertzian and the displacement of the effective pressure center from the contact center is indicated by δ_x.

In most forms of traction drives, not all of the velocities occur at once and in most cases $\Delta V = V = 0$ and only slip in the rolling direction and spin are present.

The simplified contact is shown in figure 3 together with the shear strain rate distribution in the y-direction (fig. 3(b)) and in the x-direction (fig. 3(c)). From this figure it is clear that

$$\dot{e}_x = \frac{1}{2}\left(\frac{\Delta U - \omega y}{h}\right)$$

$$\dot{e}_y = \frac{1}{2}\left[\frac{\omega(x + \delta_x)}{h}\right]$$

The system of equations (2) may now be written as

$$\left.\begin{aligned} \frac{d(\tau_x/G)}{dt} + \frac{\tau_x}{\tau_e} F(\tau_e) &= \frac{\Delta U - \omega y}{h} \\ \frac{d(\tau_y/G)}{dt} + \frac{\tau_y}{\tau_e} F(\tau_e) &= \frac{\omega(x + \delta_x)}{h} \end{aligned}\right\} \qquad (3)$$

We may use the following substitutions to nondimensionalize the set of equations (3):

$$X = x/a \qquad Y = y/b \qquad \Delta X = \delta/a$$

$$Z_x = \tau_x/\bar{\tau}_o \qquad Z_y = \tau_y/\bar{\tau}_o \qquad Z_e = \tau_e/\bar{\tau}_o$$

where $\bar{\tau}_o$ is some reference stress to be defined later. From the kinematics it follows that $x = Ut$. Now, because U is constant, we obtain $dt = (a/U)\,dX$. Equation (3) may now be written in a simple nondimensional form as

$$\left.\begin{aligned} \frac{dZ_x(\bar{\tau}_o/G)}{dX} + \frac{Z_x}{Z_e} F(Z_e \cdot \bar{\tau}_o) \frac{a}{U} &= \frac{a}{U}\left(\frac{\omega\sqrt{ab}}{h}\right)\left(\frac{\Delta U}{\omega\sqrt{ab}} - Y\sqrt{k}\right) \\ \frac{dZ_y(\bar{\tau}_o/G)}{dX} + \frac{Z_y}{Z_e} F(Z_e \cdot \bar{\tau}_o) \frac{a}{U} &= \frac{a}{U}\left(\frac{\omega\sqrt{ab}}{h}\right)\frac{(X + \Delta X)}{\sqrt{k}} \end{aligned}\right\} \tag{4}$$

where $Z_e = \sqrt{Z_x^2 + Z_y^2}$ and $k \equiv b/a$ is the aspect ratio of the contact. The boundary conditions for this set of equations are

$$Z_x = Z_y = 0 \quad \text{at} \quad X = -\sqrt{1 - Y^2} \tag{5}$$

under the assumption that the shear stresses are zero in the inlet region.

NONLINEAR FUNCTION $F(\tau_e)$

With the knowledge of the nonlinear function $F(\tau_e)$, the set of equations (4) may be solved for the stresses and hence for the traction forces.

Various forms of the function $F(\tau_e)$ are possible. In reference 11 it was shown that a fairly general form of it is given by the hyperbolic sinh, namely,

$$F(\tau_e) = \frac{\tau_c}{\eta} \sinh \frac{\tau_e}{\tau_c} \tag{6}$$

where

η linear Newtonian viscosity

τ_c reference shear stress

For fluids under high pressure, such as those that occur in traction drive contacts, it is acceptable to use the limiting case of equation (6), also known as the limiting shear stress model. In mathematical form the function may be written as

$$F(\tau_e) = 0 \qquad \text{for} \qquad \tau_e < \tau_o$$

and

$$F(\tau_e) = \frac{2(\tau_{ij} \cdot \dot{e}_{ij})}{\tau_o} \qquad \text{for} \qquad \tau_e = \tau_o \tag{7}$$

where τ_o is the local limiting shear strength of the fluid.

The model was suggested in reference 1 and has been used extensively in the analysis of traction drive contacts. The advantage in using this form of the nonlinear function is that we now only have one disposable parameter. When this form of the limiting shear stress formulation is used, equations (1) reduce to the well known Prandtl-Reuss equations for elastic, perfectly plastic material.

Curves B and C in figure 4 (reproduced from ref. 11), compare actual and predicted traction behavior of a circular contact under combined spin and slip and using the elastic-plastic form of equation (1). The two parameters G and τ_o were obtained from the measured initial slope and peak traction coefficient of the zero spin traction curve A in figure 4. These were, combined with the kinematic information on the strain distribution, used to predict the combined spin and slip curves B and C. The results show that the elastic-plastic form of equation (1) indeed predicts the observed traction correctly.

VARIATION OF THE FLUID PROPERTIES WITH PRESSURE

In order to solve equations (4) we have to know something about the effect of pressure on the magnitude of both the shear modulus G and the limiting shear stress τ_o. A simple approach would be to ignore any variation of the G and τ_o due to pressure and to set $G = \overline{G}$ and $\tau_o = \overline{\tau}_o$ where the bar denotes average properties; however, it was shown in reference 5 that to a fair approximation both G and τ_o are linear functions of pressure and, therefore a better description of the two parameters over the contact area would be to let

$$\tau_o = \frac{3}{2} \tau_o \sqrt{1 - X^2 - Y^2}$$

and

$$G = \frac{3}{2} \overline{G} \sqrt{1 - X^2 - Y^2} \tag{8}$$

This latter type of variation of G and τ_o does not necessarily give the best predictions of traction as is shown in figure 5. Here both types of variations of G and τ_o are shown. It may be observed that for small values of spin, the traction is predicted better by the averaged properties τ_o and $\overline{G}$ over the contact area, while at the larger values of spin the property variation as shown in equation (8) gives better results. Also, it should be noted that the small strain results are predominantly elastic and hence governed by G, while the large strain results are mostly governed by the plastic properties τ_o of the liquid. Therefore the following variations of G and τ_o should be used if a better fit is wanted:

$$G = \overline{G}$$

$$\tau_o = \frac{3}{2} \overline{\tau}_o \sqrt{1 - X^2 - Y^2}$$

The main reason for the apparent contradiction in the experimental variation of G with pressure and the variation giving the best fit is thought to be caused by disk compliance which is discussed in appendix A. When the present analysis is used to predict the performance of traction drive contacts consisting of the lubricant and the disks, then the appropriate value of G to use is that for the system, not just the fluid. This system modulus $\overline{G}$ can be taken as the shear modulus of the lubricant to give nearly correct predictions.

The shear modulus $\overline{G}$ and the limiting shear stress $\overline{\tau}_o$ are parameters that are not readily available but can easily be obtained from experimental traction curves. The measured initial traction slope m and the peak traction coefficient μ (see fig. 6) from a pure slip traction curve can be used to calculate $\overline{G}$ and the limiting shear stress $\overline{\tau}_o$; thus,

$$\bar{G} = \frac{3}{8} m \left(\frac{Nh}{a^2 b}\right)$$

$$\bar{\tau}_o = \frac{\mu N}{\pi ab} \qquad (10)$$

It is important that these two parameters are obtained under identical operating conditions to those prevailing in the traction drive contacts, namely contact pressure, temperature and area, film thickness and speed. It is possible, however, to use data that was obtained at the same pressure, temperature and speed but at different contact area, aspect ratio and film thickness through the use of the analysis as outlined in appendix B.

For ease of notation, various nondimensional groups are introduced now. The nondimensional groups are expressed in both the fluid properties $\bar{G}$ and $\bar{\tau}_o$ and the traction curve parameters m and μ. They are

$$J_1 = \frac{\bar{G}\sqrt{ab}}{\bar{\tau}_o h} \frac{\Delta U}{U}$$

$$= \frac{3}{8} \pi \left(\frac{m}{\mu}\right) \cdot \left(\frac{\Delta U}{U}\right) \cdot \sqrt{k} \qquad \text{(dimensionless slip)} \qquad (11)$$

and

$$J_3 = \frac{\bar{G}\sqrt{ab}}{\bar{\tau}_o h} \cdot \frac{\omega \sqrt{ab}}{U}$$

$$= \frac{3}{8} \pi \left(\frac{m}{\mu}\right) \cdot \left(\frac{\omega \sqrt{ab}}{U}\right) \cdot \sqrt{k} \qquad \text{(dimensionless spin)} \qquad (12)$$

Equations (4) and (7) may now be written as

$$\left.\begin{aligned} \frac{dZ_x}{dX} &= \frac{J_3}{\bar{k}}\left(\frac{J_1}{J_3} - Y\sqrt{\bar{k}}\right) - \left(\bar{F}(Z_e) \cdot \frac{Z_x}{Z_e}\right) \\ \frac{dZ_y}{dX} &= \frac{J_3}{k}(X + \Delta X) - \left(\bar{F}(Z_e) \cdot \frac{Z_x}{Z_e}\right) \end{aligned}\right\} \tag{13}$$

where

$$Z_e = \sqrt{Z_x^2 + Z_y^2}$$

and $\bar{F}(Z_e) = 0$ when $Z_e < \frac{3}{2}\sqrt{1 - X^2 - Y^2}$

or

$$\bar{F}(Z_e) = \frac{J_3}{Z_e\sqrt{\bar{k}}}\left[\left(\frac{J_1}{J_3} - Y\sqrt{\bar{k}}\right)Z_x + \frac{(X + \Delta X)Z_y}{\sqrt{\bar{k}}}\right]$$

when

$$Z_e = \frac{3}{2}\sqrt{1 - X^2 - Y^2}$$

Equation (13) may be solved for Z_x and Z_y using various values of J_1, J_3, k, and ΔX. In the reported calculations ΔX has been kept zero.

RIGID-PLASTIC MODEL

A particularly interesting case exists for equation (13) when the shear modulus goes to infinity and the constitutive equation reduces to that for a rigid-plastic model. The equations now represent the von Mises criteria for plastic flow. This model has been used quite frequently in traction drive analyses for example by Wernitz in reference 9 and more recently by Magi in reference 10. The resulting stress equations for this model are

$$\left.\begin{aligned} Z_x &= \frac{3}{2}\frac{\sqrt{1 - X^2 - Y^2}\ (\varepsilon - Y\sqrt{k})}{\varphi} \\ Z_y &= \frac{3}{2}\frac{\sqrt{1 - X^2 - Y^2}\ (X + \Delta X)}{\varphi\sqrt{k}} \end{aligned}\right\} \qquad (14)$$

where

$$\varphi \equiv \sqrt{(\varepsilon - Y\sqrt{k})^2 + \frac{(X + \Delta X)^2}{k}}$$

and

$$\varepsilon \equiv \frac{J_1}{J_3}$$

The parameter ε has a special meaning in traction drive analysis and is often referred to as the speed pole location. Its meaning is made clear by looking at figure 3(c) where e is given by $e = \Delta U/\omega$. If we now divide this by $\sqrt{ab}$, we obtain $e/\sqrt{ab} \equiv \varepsilon = \Delta U/\omega\sqrt{ab}$. So the speed pole location parameter ε is nothing more than the ratio of slip to spin in the contact. This speed pole parameter is identical to that used by Magi in reference 10. From the definition of J_1 and J_3 we find that $\varepsilon \equiv J_1/J_3$. Strictly speaking the parameter J_1 and J_3 should not be used for the rigid-plastic model because both contain the shear modulus, however, the ratio J_1/J_3 forms a convenient independent parameter that is consistent with the work of previous researchers. Equation (14) then, is a limiting form of equation (13) when the elastic effects are negligible with J_1/J_3 as one of the independent parameters.

TRACTION CALCULATIONS

Of real interest in traction drive design are the traction, the slip, and the total losses in the system. Also of concern is the degree of sophistication that should be used to obtain correct answers. The level of the analysis is dependent upon where the elastic properties of the fluid are important and when the plastic properties are more dominant. These questions may be answered by solving equation (13) for the traction parameters.

In terms of the nondimensional parameters we have for the traction forces

$$\left.\begin{aligned} F_x &= \int_A \tau_x dA = ab\bar{\tau}_o \int_A Z_x dX\, dY \\ &= \pi ab\bar{\tau}_o J_4 \end{aligned}\right\} \quad (15)$$

where

$$J_4 \equiv \frac{1}{\pi} \int_A Z_x dX\, dY = \text{nondimensional traction in the rolling direction}$$

$$= \frac{F_x}{\pi ab\bar{\tau}_o} = \frac{F_x}{\mu N}$$

Similarly,

$$J_5 \equiv \frac{F_y}{\pi ab\bar{\tau}_o} = \frac{F_y}{\mu N} = \text{nondimensional traction perpendicular to the rolling direction.}$$

For the torque on the spinning contact we have

$$T = \int_A (\tau_y \cdot x - \tau_x \cdot y) dA$$

or

$$\frac{T}{\bar{\tau}_o ab\pi \cdot \sqrt{ab}} = \frac{T}{\mu N \cdot \sqrt{ab}} = J_6 \quad (16)$$

where

$$J_6 \equiv \frac{\sqrt{k}}{\pi} \int_A (Z_y \cdot X - Z_x \cdot Y \cdot k) dX\, dY$$

The power dissipated in the contact can now be calculated in terms of these nondimensional parameters; namely,

$$J_7 = J_6 \cdot J_3 + J_4 \cdot J_1$$

or in terms of real power

$$J_7 = \frac{\bar{G}}{\pi\sqrt{ab}\tau_o^2 hU} (T \cdot \omega + F_x \cdot \Delta U)$$

or

$$J_7 = \frac{3\pi}{8U} \cdot \sqrt{k} \cdot \frac{m}{\mu^2 N} (T \cdot \omega + F_x \cdot \Delta U) \qquad (17)$$

where the terms in parentheses are the individual components of the power loss due to spin and longitudinal slip.

The important information from the calculations to present are traction J_4, J_5, and torque J_6 as functions of slip J_1 and spin J_3. Any other quantity may be calculated from these five parameters. As an independent variable we may select slip J_1, based upon the elastic-plastic argument, or the speed pole location J_1/J_3 as found in the rigid-plastic analysis. For the traction in the rolling direction J_4 it was decided to present the data using both slip J_1 and speed pole locations J_1/J_3 as the independent variable since both types of graphs reveal significant information.

The zero spin traction curves for an elastic-plastic material at various aspect ratios are shown in figure 7. We observe that at any slip J_1 we obtain more traction J_4 with the lower aspect ratio contacts. The explanation of this behavior lies in the fact that the mean shear strain is directly proportional to the contact dimension in the X-direction. The lower aspect ratio contacts have their semimajor axis in the running direction and therefore see a larger mean shear strain and hence the mean shear stress is larger. The effect shows up in the traction.

It may be expected that, at high local strain rates, the elastic effects are not significant and that the rigid-plastic model may be used to solve for the tractions. Figure 8 shows the traction J_4 for the rigid-plastic model at various aspect ratios as a function of the speed pole location. Again lower aspect ratio contacts appear to have a slight edge on traction for the same speed pole parameter.

To observe the effect of spin J_3 on the traction J_4 for the elastic-plastic model, the traction J_4 was calculated with various values of spin J_3 present and the results are shown in figure 9. These results are also presented with the speed pole parameter as the independent parameter in figure 10. A simple comparison with figures 7 and 8 therefore will show the influence of both elastic effects and spin on the traction J_4. In each case the connected lines represent constant values of spin J_3.

Figure 11 shows the resulting side force traction J_5 for $k = 1$ when a contact is under spin. This force is the result of elastic behavior of the fluid under spin and slip. At low slip $J_1 < 1.0$, the side force J_5 starts at zero for zero spin, reaches a maximum and then decreases for increasing spin. When more slip J_1 is introduced, the behavior is altered somewhat and the maximum value diminishes. Figure 12 shows the variation of the maximum value of the side force J_5 as a function of the aspect ratio k. Generally when k is small, there are larger side forces. As can be seen from figure 12 the side force J_5 can be an appreciable fraction of the traction J_4.

Figure 13 shows the values of nondimensional torque J_6 as a function of speed pole locations of J_1/J_3. Solid lines again indicate constant values of spin J_3. The resulting traction curves of J_4 versus slip J_1 (fig. 9) or speed pole location J_1/J_3 (fig. 10) show that in both cases the traction J_4 tends toward a limiting traction curve and appears to be independent of spin J_3. In figure 9 the lower spin value traction curves are indistinguishable from the zero spin traction curve. This suggests that below a certain value of spin J_3 the resulting value of traction J_4 is insensitive to spin and that the simple elastic-plastic model without spin predicts the correct tractions. From figure 10 it may be observed that for high values of spin J_3 the curves are indistinguishable from the traction curve for a rigid-plastic-like material. The suggestion here is that for values of spin J_3 above a certain threshold value the traction results J_4 are in fact independent of any elastic effects in the sheared material. This form of behavior with spin J_3 could have been predicted from the nature of the constitutive equation (13). For small values of spin J_3 the behavior would be almost elastic-like while for large values of spin J_3 the differential equations (13) become singular in nature. From all of the results in figures 9 and 10 it may be observed that the two threshold values are dependent on the ellipticity of the contact. In traction drives we are generally only interested in the traction range that lies somewhere near 75 percent of the maximum obtainable traction. For this traction value the various threshold values of spin J_3 as a function of the aspect ratio are shown in figure 14. The three regions of influence are indicated on figure 14. They are

Region I - elastic-plastic analysis without spin is sufficient

Region II - elastic-plastic analysis with spin is required

Region III - rigid-plastic analysis with spin is sufficient

The lines dividing the regions are the values of spin J_3 corresponding to a 5 percent increase in the slip traction level, compared to the master traction curves in figures 7 and 8.

LOSS FACTORS

Losses in the contacts of a traction drive are made up of two components (slip and spin losses) as was indicated in equation (17):

$$J_7 = (J_6 \times J_3 + J_4 \times J_1)$$

From the calculated results the power loss J_7 can be calculated from the individual components and we can establish curves of J_7 as a function of slip J_1 or speed pole location J_1/J_3. An example of J_7 versus J_1 is shown in figure 15 for $k = 1$.

It is, however, more convenient to define a loss factor LF which has a more direct meaning to us as follows:

$$(LF) \equiv \frac{J_7}{J_4}$$

$$= \frac{\bar{G}}{U\pi\sqrt{ab}\,\bar{\tau}_o^2 h}\,(T \cdot \omega + F_x \cdot \Delta U) \Big/ \frac{F_x}{\pi ab\bar{\tau}_o}$$

$$= \frac{\bar{G}\sqrt{ab}}{\bar{\tau}_o h}\left(\frac{\text{power loss}}{\text{power input}}\right)$$

$$= \frac{3\pi}{8}\sqrt{k}\,\frac{m}{\mu}\left(\frac{\text{power loss}}{\text{power input}}\right) \tag{18}$$

The loss factor may be thought of as an equivalent creep in the power transmission direction. It is interesting to note that, when the drive is idling (i.e., no net power output), then the loss factor is simply given by

$$(LF)_o = \frac{\bar{G}\sqrt{ab}}{\bar{\tau}_o h} \tag{19}$$

or in terms of traction curve parameters

$$(LF)_o = \frac{3\pi}{8} \sqrt{k} \frac{m}{\mu} \tag{20}$$

and we see that the idling losses are directly related to the traction curve parameters. Figure 16 shows the calculated loss factor curves as a function of the dimensionless transmitted traction J_4. This way of presenting the data is most useful since most forms of the traction drives employ a mechanism whereby the ratio of the normal load to the tractive force transmitted is maintained constant at values of 60 to 80 percent of the maximum obtainable traction coefficient. This feature means that these types of drives operate at essentially a constant value of J_4 much of the time, that is, along a vertical line at a constant value of J_4 in figure 16.

From the results in figure 16 it may be observed that the region of 60 to 80 percent of the maximum available traction, or $J_4 = 0.6$ to 0.8, is the most efficient when substantial spin is present, though this depends somewhat on the aspect ratio k. Also in this same region it may be observed that the loss factor is not affected by small values of spin and that it is the lowest for the contacts of low aspect ratio. The insensitivity to small values of spin indicates that the losses in the contact are predominantly due to creep for these small values of spin.

In figure 17 the loss factor at traction $J_4 = 0.75$ is plotted against the spin J_3 for the various aspect ratios considered in this work. From this figure it may be observed that the imposed spin has little or no influence on the loss factor at low values of spin.

From a practical point of view it can be concluded from figure 17 that a traction drive may be operated with values of spin J_3 up to approximately one without increasing the power losses in the contact.

Figure 18 shows the loss factor plotted as a function of J_1/J_3 at constant values of spin J_3 for $k = 1$. This figure indicates that the minimum value of the loss factor occurs at approximately constant values of the speed pole location ε or J_1/J_3 independent of the amount of spin present. This may be useful information in the design of angular contact bearings to minimize their losses.

CONCLUSIONS

The elastic-plastic approximation of the Johnson and Tevaarwerk fluid traction model was used to analyze the traction behavior of typical traction drive contacts. The two required fluid properties, shear modulus and limiting fluid shear strength, were allowed to vary over the contact area in accordance with observed traction behavior.

This investigation was particularly aimed at the role that both contact configuration and spin play in longitudinal traction. Graphical solutions of the analysis are provided which allow for the design optimization of traction drive contacts. Comparisons were made between the full Johnson and Tevaarwerk solutions and those which can be arrived at by using the commonly used rigid-plastic analysis due to Wernitz.

The most important conclusions drawn from the analysis are the following:

1. Under conditions of slip and spin several simplifications in the analysis may be used; they are (a) The influence of low spin values is negligible on the traction. Simple slip analysis with the elastic-plastic model is sufficient. (b) At moderate values of spin the complete analysis of spin with the elastic-plastic model is needed to give accurate traction predictions. (c) At high values of spin the elastic effects in the fluid may be neglected and the simple rigid-plastic analysis due to Wernitz may be used.

2. Traction improves with contacts whose major axis is in the rolling direction.

3. Sideways forces due to the spin on the contact can be a substantial fraction of the transmitted traction.

4. The effect of spin is always deleterious to traction efficiency.

Lewis Research Center,
National Aeronautics and Space Administration,
Cleveland, Ohio, July 11, 1979,
511-58.

APPENDIX A

CORRECTIONS FOR DISK COMPLIANCE

One of the implicit assumptions made in the present analysis is that the two contacting bodies are infinitely stiff in the plane of contact. This is not so in many practical situations. The effect of disk compliance may be studied by the following very simple model. Consider the layer of film between the two "contacting" disks. The combination disk, film, disk form a sandwich of three deformable elements and relative velocities between the two disks is accommodated by shear in all three elements. When the film is thin and stiff, most of the shear may in fact take place in the disks. This is certainly the case when the disks roll together without a lubricant. For two bodies that roll together without a lubricant film it has been shown in references 12 and 13 that the following creep due to the transmitted traction force F occurs:

$$\left(\frac{\Delta U}{U}\right)_{dry} = q\left(\frac{F}{\pi a b G_s}\right) \tag{A1}$$

where

G_s shear modulus of disk material

q constant depending on aspect ratio (given in appendix B).

For an elastic lubricant film of thickness h under shear due to the transmitted traction force F the creep is given by

$$\left(\frac{\Delta U}{U}\right)_{film} = \frac{32}{9\pi}\frac{h}{a}\left(\frac{F}{\pi a b \bar{G}}\right) \tag{A2}$$

where it was assumed that

$$G = \frac{3}{2}\bar{G}\sqrt{1 - X^2 - Y^2} \tag{8}$$

The total creep for the sandwich under the imposed traction F is given by the sum of the disk creep and the film creep, namely,

$$\left(\frac{\Delta U}{U}\right)_{total} = \frac{F}{\pi a b}\left(\frac{q}{G_s} + \frac{32}{9\pi}\frac{h}{a}\frac{1}{G}\right) \tag{A3}$$

The parameter q covers the range of $q = 0.4$ for $k = 0.2$ to $q = 0.93$ for $k = 5$ (longitudinal creep only). For commonly used traction drives operating at pressures above 1.2 gigapascals, $h/a \simeq 10^{-3}$ and steel is generally employed as the disk material. When these values are used in equation (A3) together with a fluid shear moduli $\bar{G}$ of about 10^9 pascals, as found experimentally, then it is observed that most of the creep in the sandwich in the small slip region takes place in the disks, not in the fluid film. Reported shear moduli, as obtained from disk machine experiments have to be corrected for this effect (see, for example, refs. 5, 11, 14, and 15) for compliance corrected shear moduli.

If, in the region of operation of traction drives, most of the elastic effects are caused by the disk material, then we are justified in using the shear modulus as a constant over the contact area since G_s is not affected to any extent by the normal pressure.

APPENDIX B

CORRECTIONS FOR CONTACT AREA, ASPECT RATIO, AND FILM THICKNESS

Frequently traction data is available for a fluid at the same speed, temperature, and pressure but not at the same contact area because the roller geometry may have been different. From the analysis in the text it is clear that roller compliance and contact area play a significant role in the determination of the traction slope. An exact analysis for the correction of these terms is not yet possible; however, we can attempt the following simplified procedure.

If we let m' be the slope of the traction curve for dry rolling bodies, then it follows that the compliance corrected modulus for the fluid is approximately

$$G_c = \bar{G}\left(1 - \frac{m}{m'}\right)^{-1} \tag{B1}$$

where

G_c compliance corrected modulus

$\bar{G}$ apparent modulus

m wet slope for contact

m' dry slope for contact

From the main text we have an expression for the apparent modulus equation

$$G = \frac{3}{8} m\left(\frac{Nh}{a^2 b}\right) \tag{10}$$

Also from equation (A1), we have for the dry slope that

$$\frac{F}{N}\Big/\frac{\Delta U}{U} \equiv m' = \frac{\pi ab G_s}{qN} \tag{B2}$$

Now because $N = (2/3)\,\pi ab P_o$ we can simplify this equation a bit further to

$$m' = \frac{3}{2}\frac{G_s}{qP_o} \tag{B3}$$

where q is aspect ratio dependent. Also equation (10) may be put in a slightly simpler form by this method

$$\overline{G} = \frac{\pi}{4} m \frac{P_o h}{a} \tag{B4}$$

If we now assume that the compliance correction according to equation (B1) is good to a fair degree, then for different measurements at the same pressure, speed, and temperature we might at least expect that the compliance corrected modulus would be the same; or if the * parameters refer to one set of experiments and the nonsuperscripted parameters to another set, then we may write under the aforementioned assumptions the following:

$$G_c = G_c^*$$

By using equations (B1) and (B4) this becomes

$$\frac{\pi}{4} m \frac{P_o h}{a} \left(1 - \frac{m}{m'}\right)^{-1} = \frac{\pi}{4} \frac{m^* h^*}{a^*} P_o \left(1 - \frac{m^*}{m'^*}\right)^{-1} \tag{B5}$$

The comparison is made at the same pressure P_o so we can simplify the aforementioned expression to

$$\frac{m^* h^* a}{m h a^*} = \left[1 + \frac{m}{m'} \left(\frac{a^* h m'}{m'^* h^* a} - 1\right)\right]^{-1} \tag{B6}$$

From equation (B3) for the same material and contact pressure we can write $m'/m'^* = q^*/q$ so that the final form of equation (B6) is

$$\frac{m^* h^* a}{m h a^*} = \left[1 + \frac{2}{3} \frac{m q P_o}{G_s} \left(\frac{a^* h q^*}{a q h^*} - 1\right)\right]^{-1} \tag{B7}$$

Equation (B7) now relates the unknown slope m^* to the other known parameters.

We do need the parameters q (the Kalker coefficients). These may be obtained from reference 13, and are plotted for both longitudinal traction measurements q_x and side slip traction measurements q_y in figure 19.

Equation (B7) is plotted in figure 20 for a common range of variables.

REFERENCES

1. Clark, O. H.; Woods, W. W.; and White, J. R.: Lubrication at Extreme Pressure with Mineral Oil Films. J. Appl. Phys., vol. 22, no. 4, Apr. 1951, pp. 474-483.
2. Smith, F. W.: The Effect of Temperature in Concentrated Contact Lubrication. ASLE Trans., vol. 5, no. 1, Apr. 1962, pp. 142-148.
3. Crook, A. W.: The Lubrication of Rollers, IV: Measurement of Friction and Effective Viscosity. Phil. Trans. Roy. Soc. (London), Series A, vol. 255, 1963, pp. 281-312.
4. Johnson, K. L.; and Cameron, R.: Shear Behavior of Elastohydrodynamic Oil Films at High Rolling Contact Pressures. Proc. Inst. Mech. Eng. (London), vol. 182, pt. I, no. 14, 1967, pp. 307-319.
5. Johnson, K. L.; and Tevaarwerk, J. L.: Shear Behavior of Elastohydrodynamic Oil Films. Proc. Roy. Soc. (London), Series A, vol. 356, no. 1685, Aug. 24, 1977, pp. 215-236.
6. Bridgeman, P. W.: Effect of Pressure on the Viscosity of 43 Pure Liquids. Proc. Am. Acad. Arts Sci., vol. 61, 1926, pp. 57-99.
7. Pressure Viscosity Report, Vols. 1 and 2. American Society of Mechanical Engineers, 1953.
8. Fein, R. S.: Effects of Lubricants on Transition Temperatures. ASLE Trans., vol. 8, no. 1, Jan. 1965, pp. 59-68.
9. Wernitz, W.: Friction at Hertzian Contact with Combined Roll and Twist. Rolling Contact Phenomena, J. B. Bidwell, ed., Elsevier Publ. Co., Inc., 1962, pp. 132-156.
10. Magi, Mart: On Efficiencies of Mechanical Coplanar Shaft Power Transmissions. Chalmers University of Technology, Gothenburg, 1974.
11. Tevaarwerk, J. L.: The Shear of Elastohydrodynamic Oil Films. Ph. D. Dissertation, Univ. of Cambridge, 1976.
12. Johnson, K. L.: The Effect of Spin Upon the Rolling Motion of an Elastic Sphere on a Plane. J. Appl. Mech., vol. 25, no. 3, Sep. 1958, pp. 332-338.
13. Kalker, J. J.: On the Rolling Contact of Two Elastic Bodies in the Presence of Dry Friction. Ph. D. Dissertation, Technische Hogeschool, Delft, 1967.

14. Johnson, K. L.; and Roberts, A. D.: Observations of Viscoelastic Behavior of an Elastohydrodynamic Lubricant Film. Proc. Roy. Soc. (London), Series A, vol. 337, no. 1609, Mar. 19, 1974, pp. 217-242.

15. Johnson, K. L.; Nayak, L.; and Moore, A. J.: Determination of Elastic Shear Modulus of Lubricants from Disc Machine Tests. Presented at the 5th Leeds-Lyon Symposium on Tribology: "Elastohydrodynamics and Related Topics," (Leeds, England), Sep. 19-22, 1978, Paper 21.

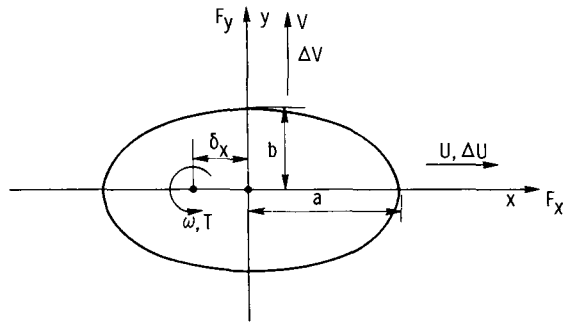

Figure 1. - Plan view of typical EHL contact indicating major variables; x is rolling direction. (The semimajor and minor axis are calculated from Hertzian theory.)

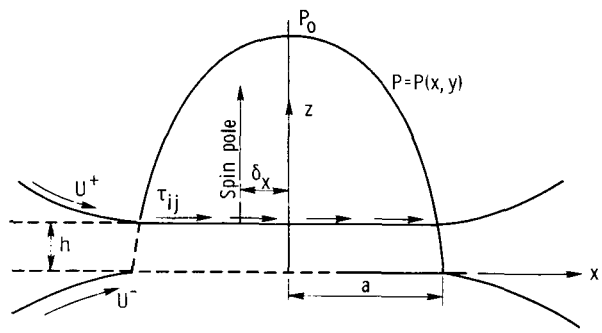

Figure 2. - Sideview of typical EHL contact with constant separation between two contacting bodies. Pressure distribution in contact area is assumed to be Hertzian.

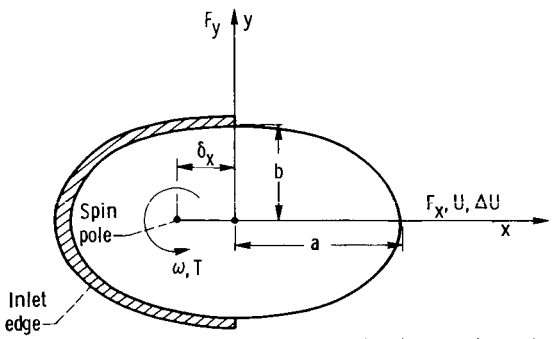

(a) Plan view of typical EHL contact showing inlet regions where shear stresses are assumed to be zero.

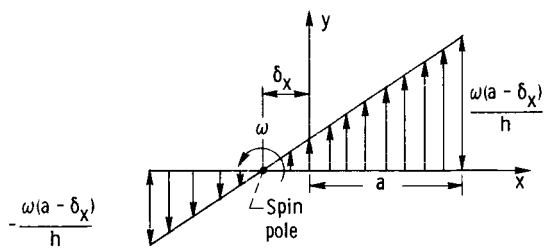

(b) Assumed shear strain rate distribution in y-direction along x-axis to spin and spin pole offset.

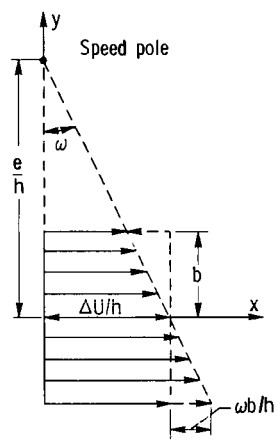

(c) Assumed shear strain rate distribution along y-axis in rolling direction due to spin and slip. Note location of speed pole $e \cong \Delta U/\omega$.

Figure 3. - Plan view of typical EHL contact with its associated center line strain rate distribution due to slip, spin, and spin pole offset.

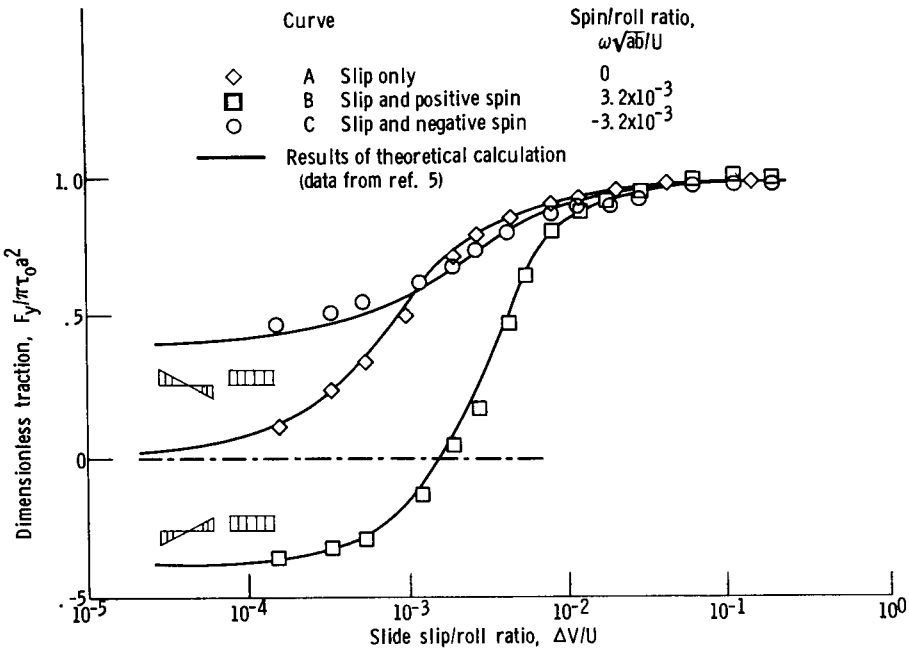

Figure 4. - Tests on hydratorque medium fluid in combined side slip and spin. Velocity in x-direction U = 1.9 meters per second; maximum Hertzian pressure in contact P_0 = 1.3 gigapascals; inlet temperature, 17° C. Elastic-plastic theory fitted to experimental results.

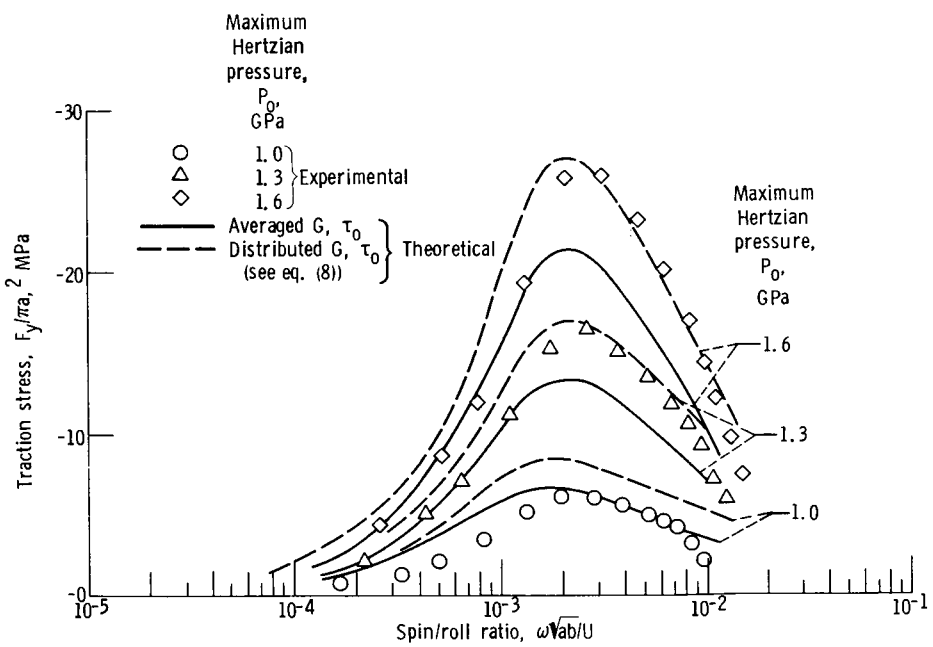

Figure 5. - Influence of average and pressure dependent shear properties G and τ_0 on spin fraction prediction (data from ref. 5). Fluid, Turbo 33; velocity in x-direction U = 1.2 meters per second; inlet temperature, 30° C.

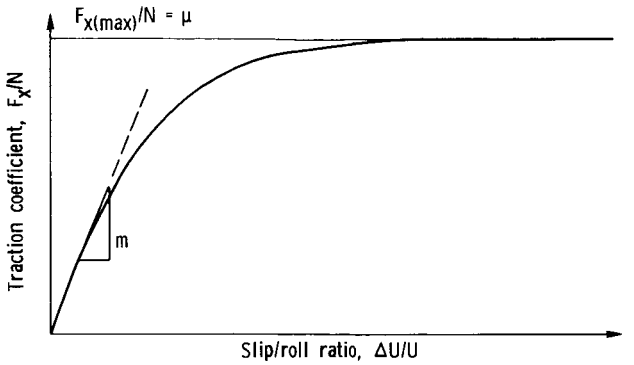

Figure 6. - Typical traction curve showing maximum traction coefficient μ and traction slope m.

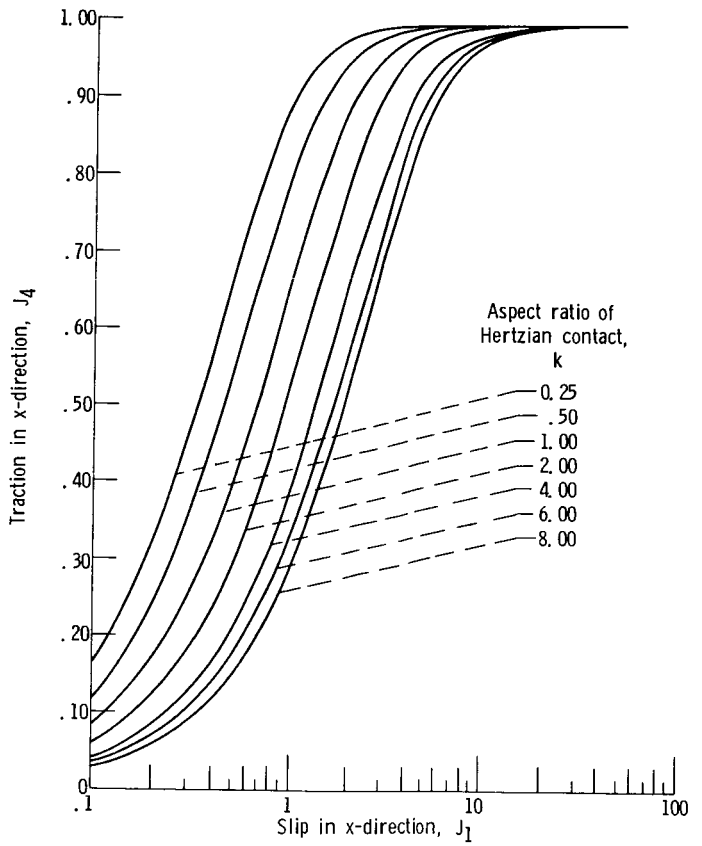

Figure 7. - Traction J_4 versus slip J_1 for various aspect ratios. Elastic-plastic theory is used. Dimensionless spin $J_3 = 0$; dimensionless spin pole offset $\Delta x = 0$.

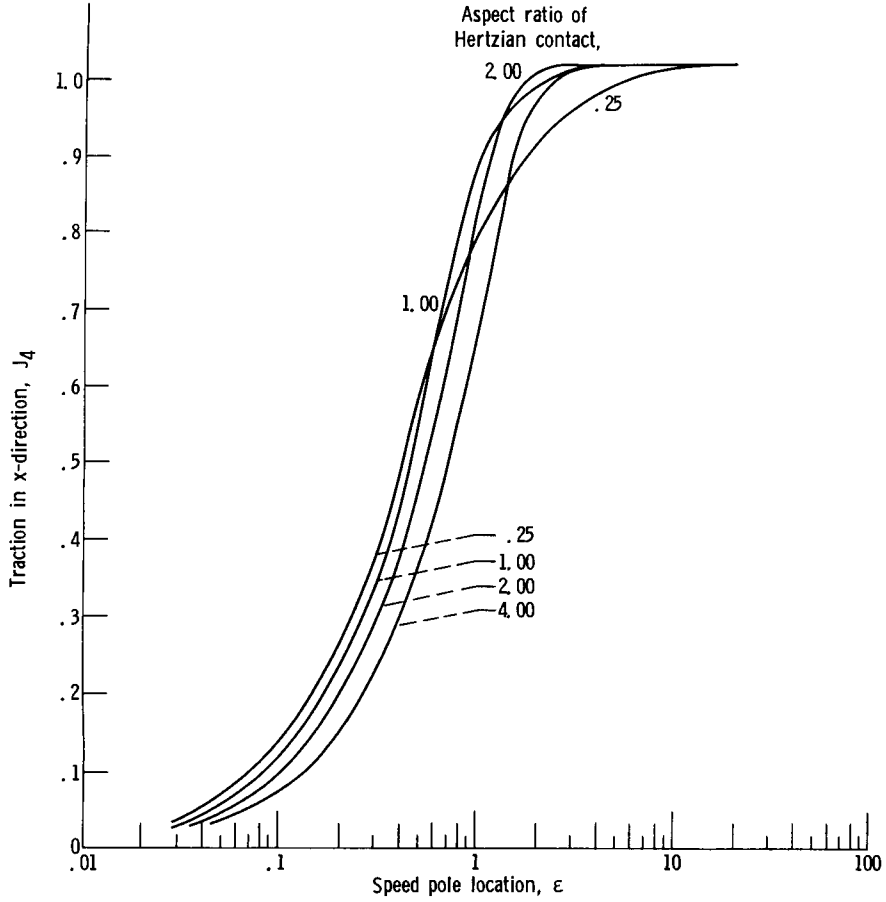

Figure 8. - Traction J_4 versus speed pole location for various aspect ratios. Rigid perfect plastic theory is used. Dimensionless spin pole offset $\Delta x = 0$.

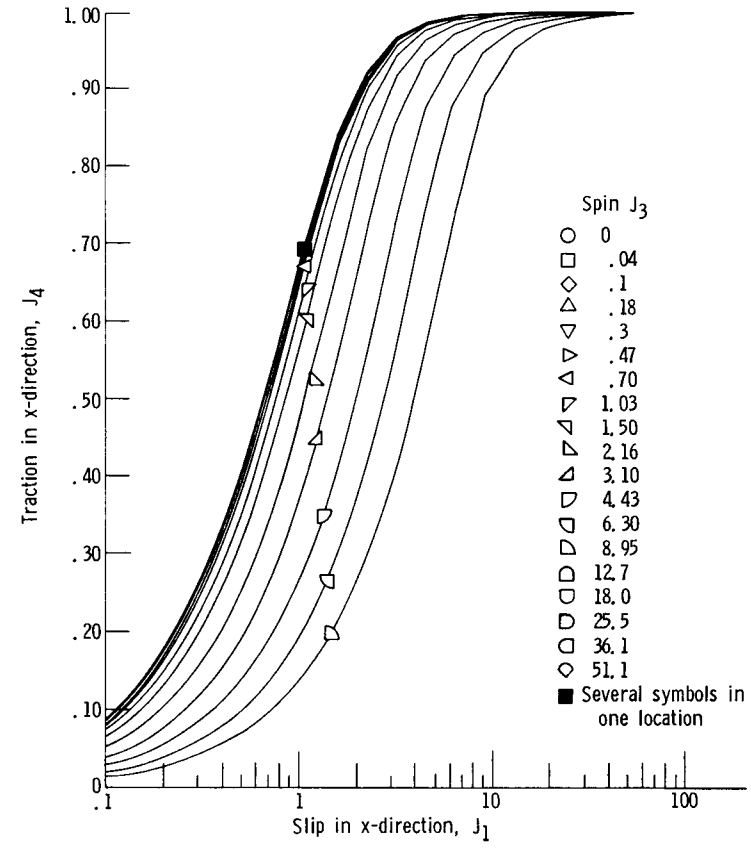

(a) Aspect ratio of Hertzian contact k = 1.00.

Figure 9. - Traction J_4 versus slip J_1 at various spin J_3 values.

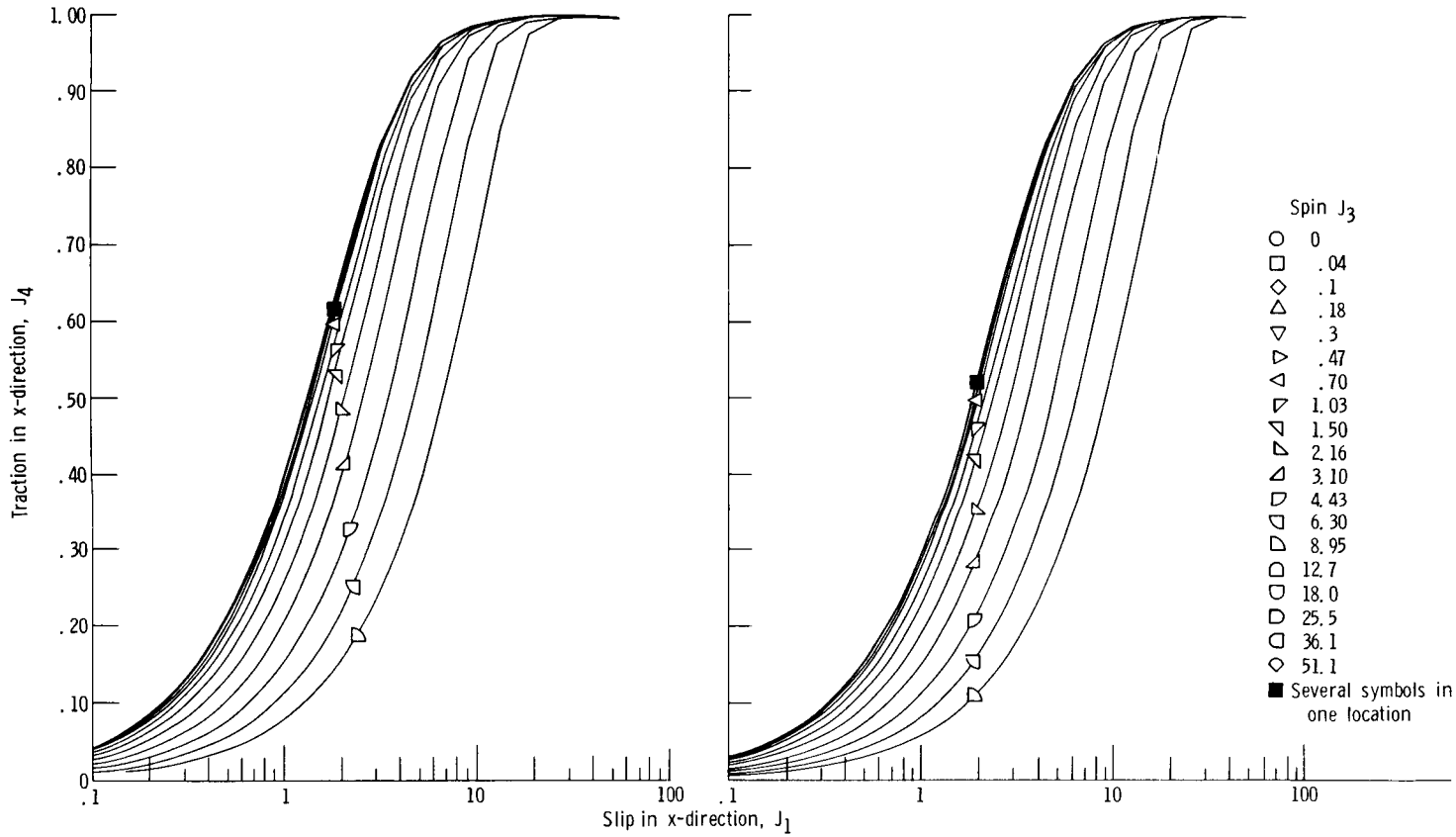

(b) Aspect ratio of Hertzian contact k = 4.00.

(c) Aspect ratio of Hertzian contact k = 8.00.

Figure 9. - Concluded.

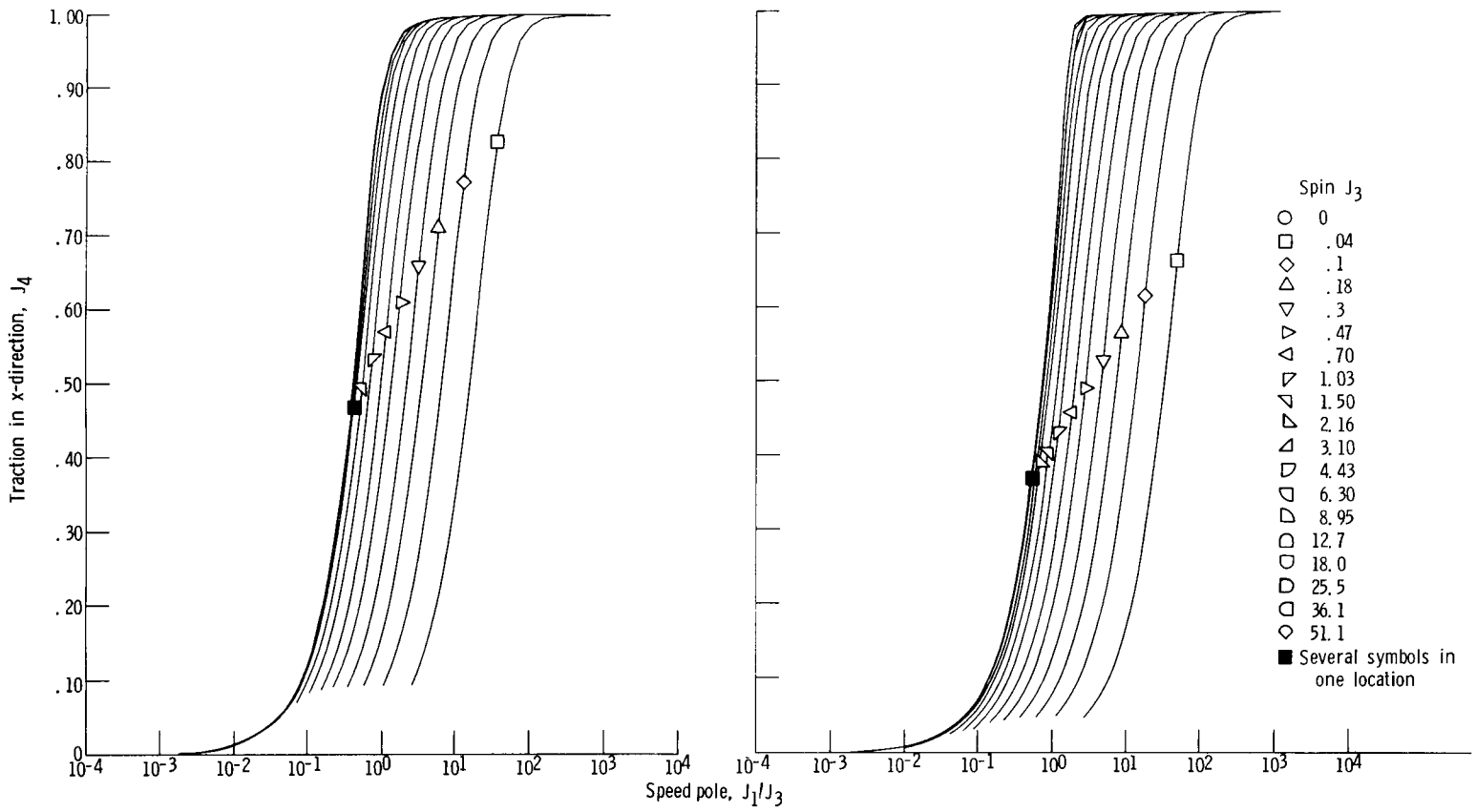

(a) Aspect ratio of Hertzian contact k = 1.00.

(b) Aspect ratio of Hertzian contact k = 4.00.

Figure 10. - Traction J_4 versus speed pole location ϵ, (J_1/J_3) at various spin values.

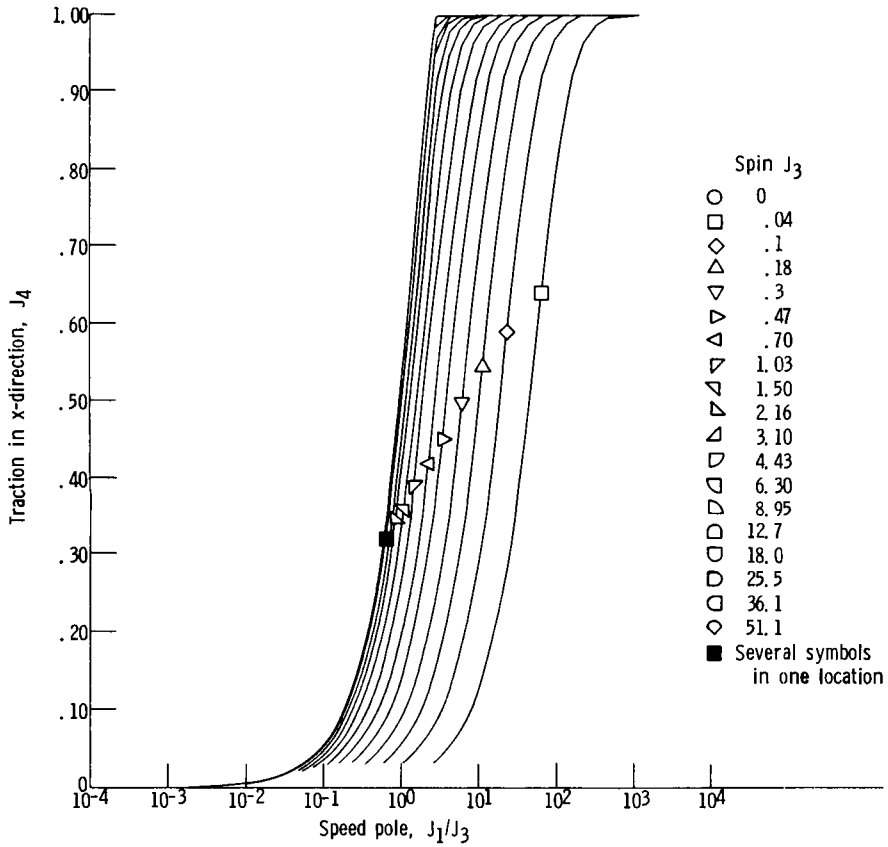

(c) Aspect ratio of Hertzian contact k = 8.00.

Figure 10. - Concluded.

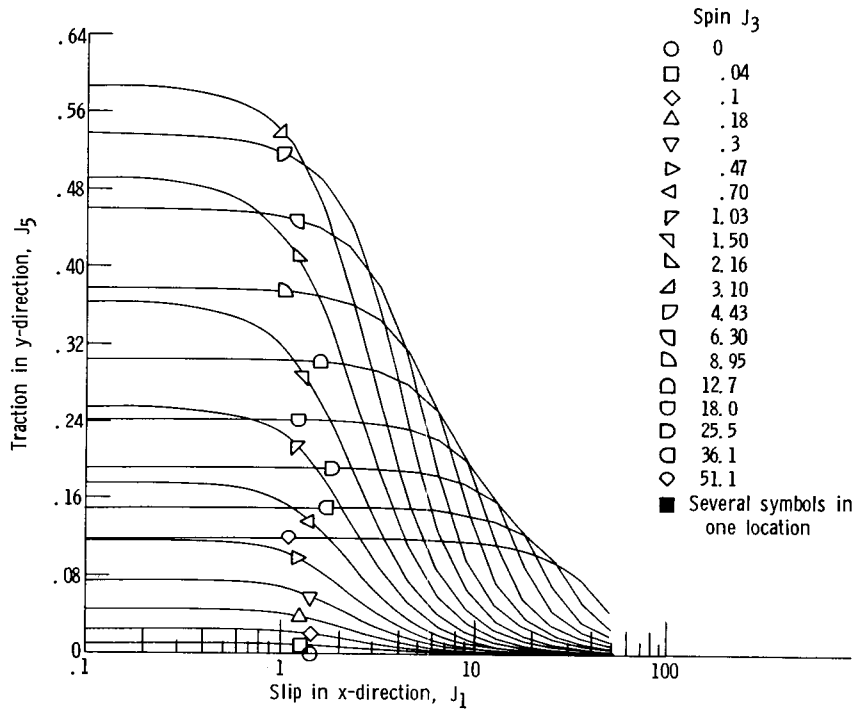

Figure 11. - Traction J_5 versus slip J_1 at various values of spin J_3. Aspect ratio of Hertzian contact k = 1.00.

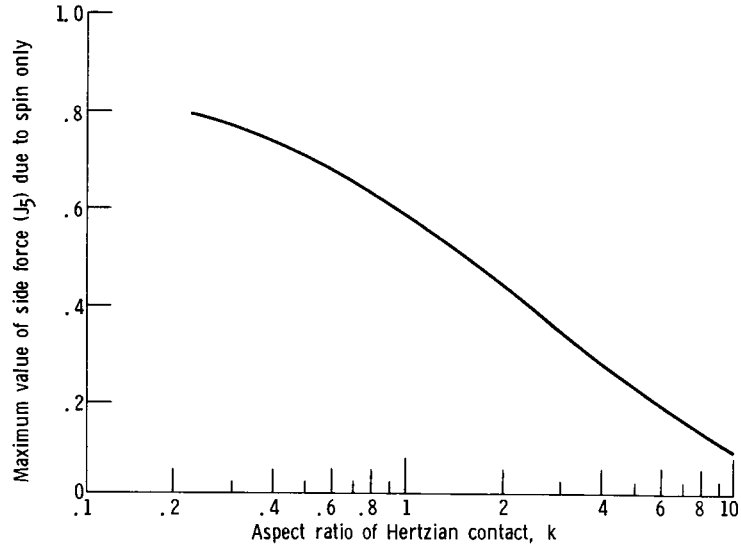

Figure 12. - Variation of maximum side force (J_5) with aspect ratio for contact under spin only.

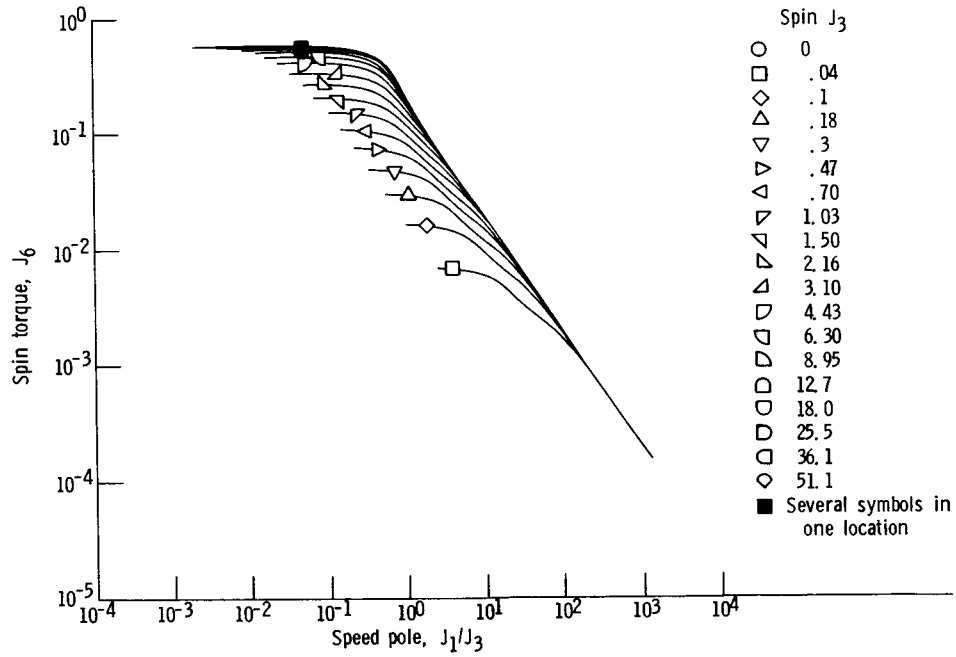

(a) Aspect ratio of Hertzian contact k = 1.00.

Figure 13. - Dimensionless spin torque J_6 versus the speed pole location J_1/J_3 at various spin J_3 values.

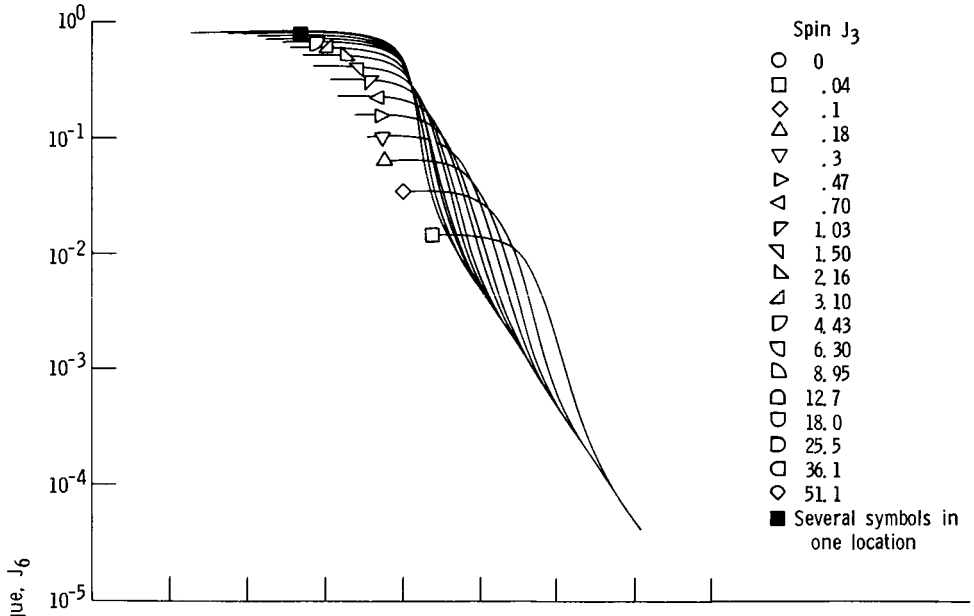

(b) Aspect ratio of Hertzian contact k = 4.00.

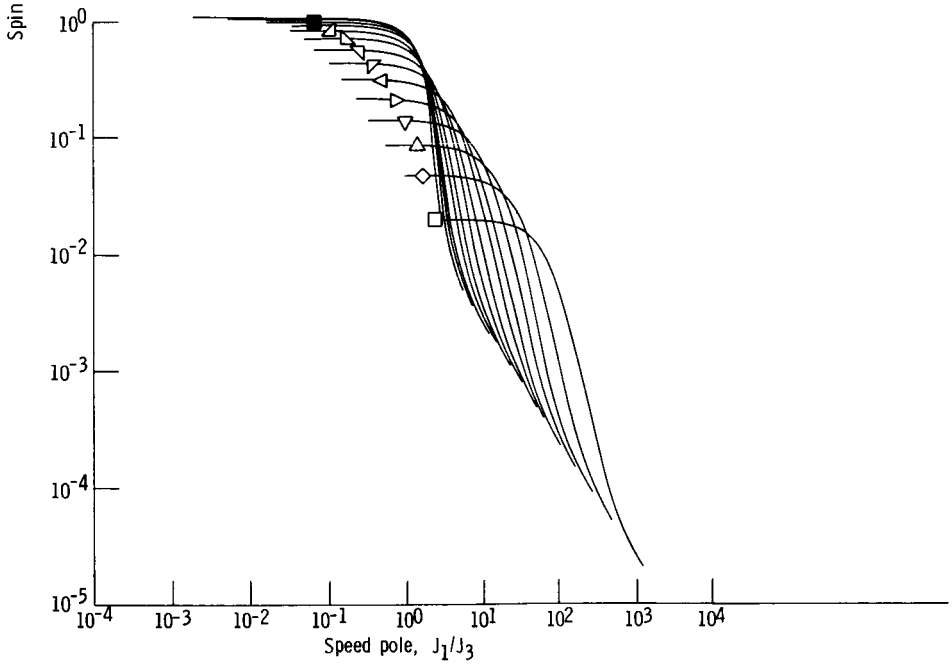

(c) Aspect ratio of Hertzian contact k = 8.00.

Figure 13. - Concluded.

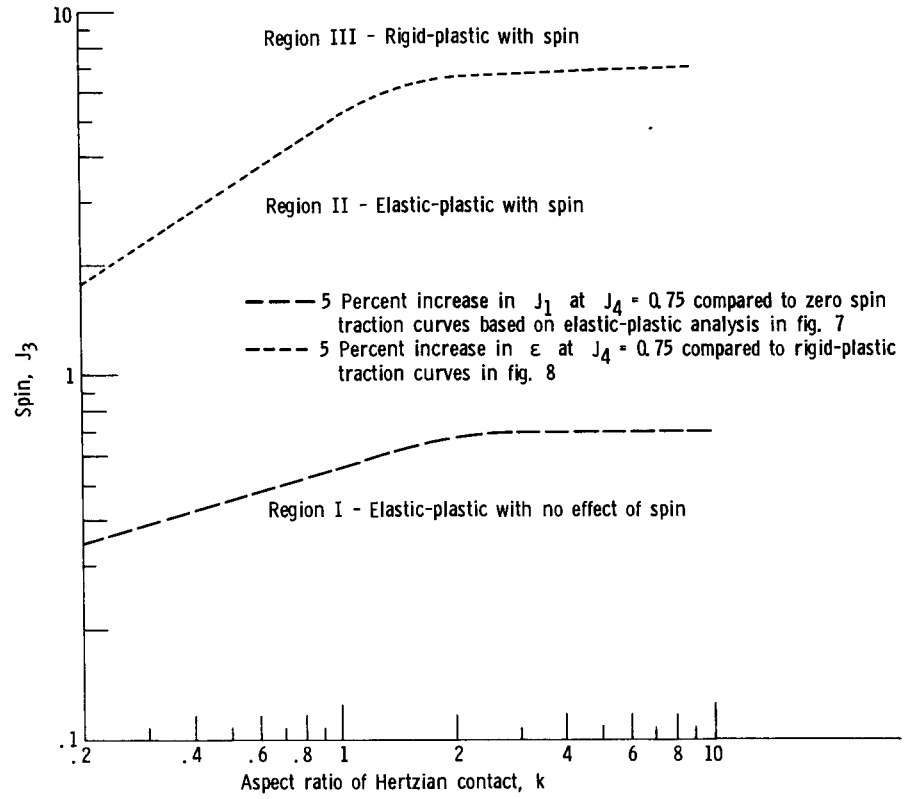

Figure 14. - Regions of influence of elastic and spin effects on slip J_1 at constant traction value J_4 = 0.75.

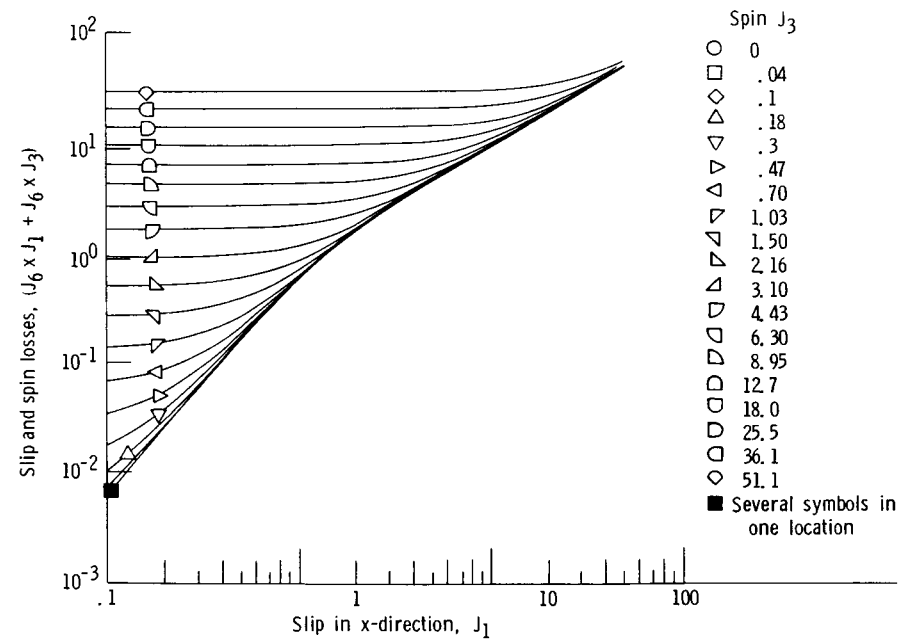

Figure 15. - Variation of $J_7 = (J_4 \times J_1 + J_6 \times J_3)$ with slip J_1 for aspect ratio of Hertzian contact k = 1.00.

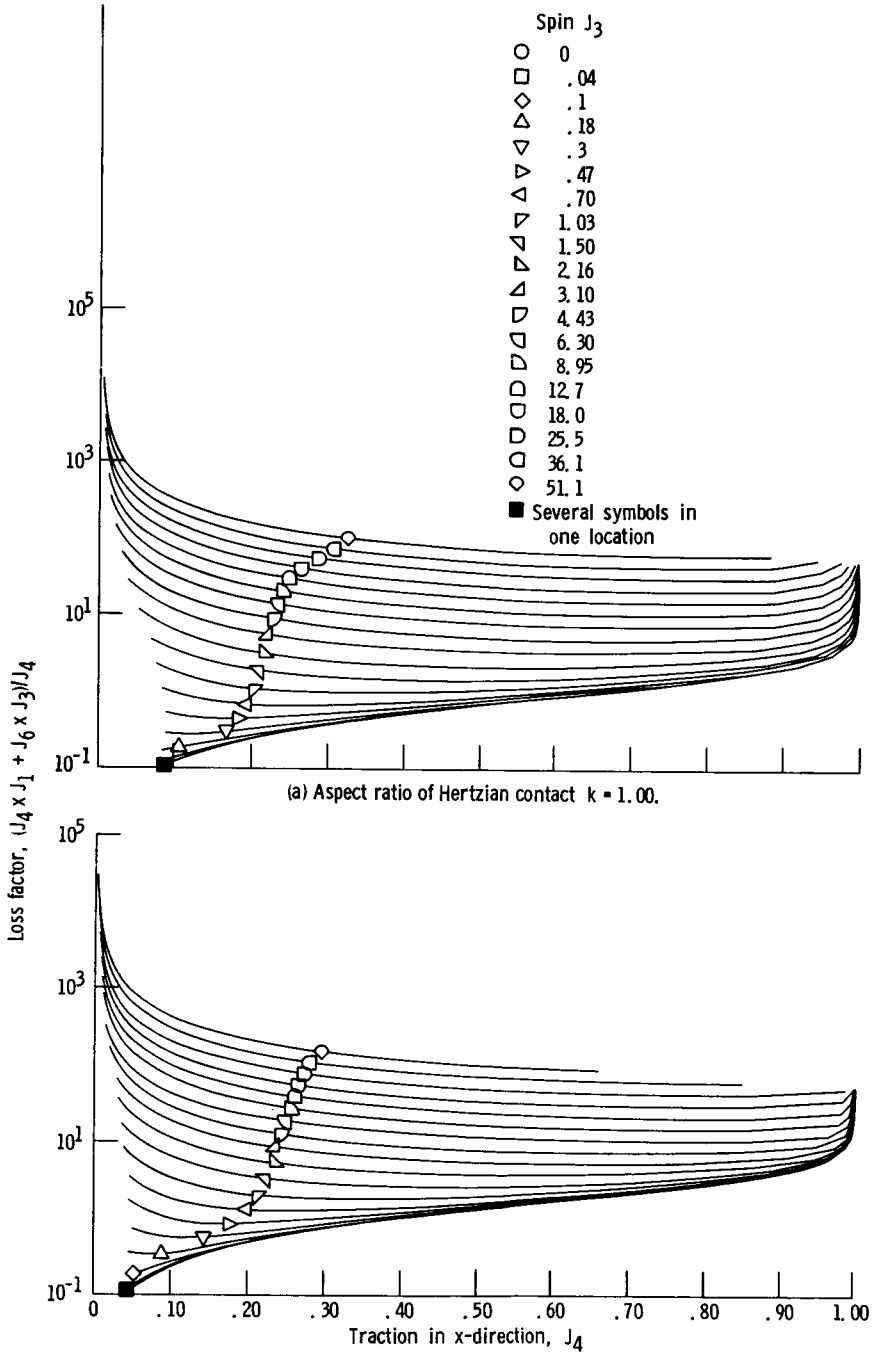

(a) Aspect ratio of Hertzian contact k = 1.00.

(b) Aspect ratio of Hertzian contact k = 4.00.

Figure 16. - Loss factor as function of traction J_4 at various spin J_3 values.

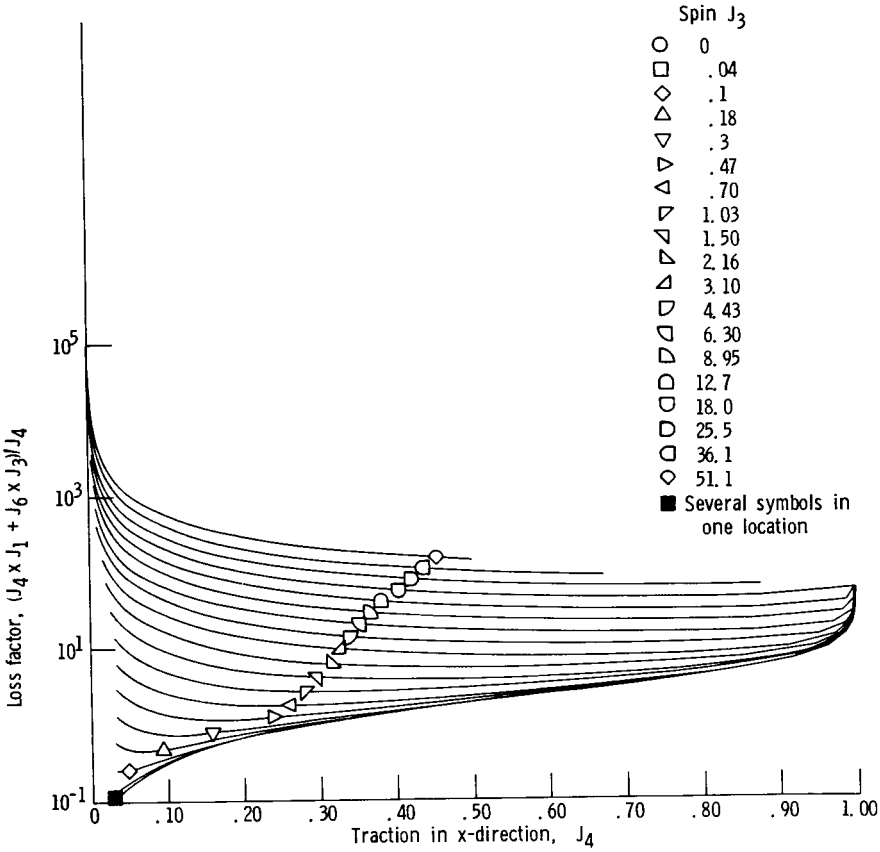

(c) Aspect ratio of Hertzian contact k = 8.00.

Figure 16. - Concluded.

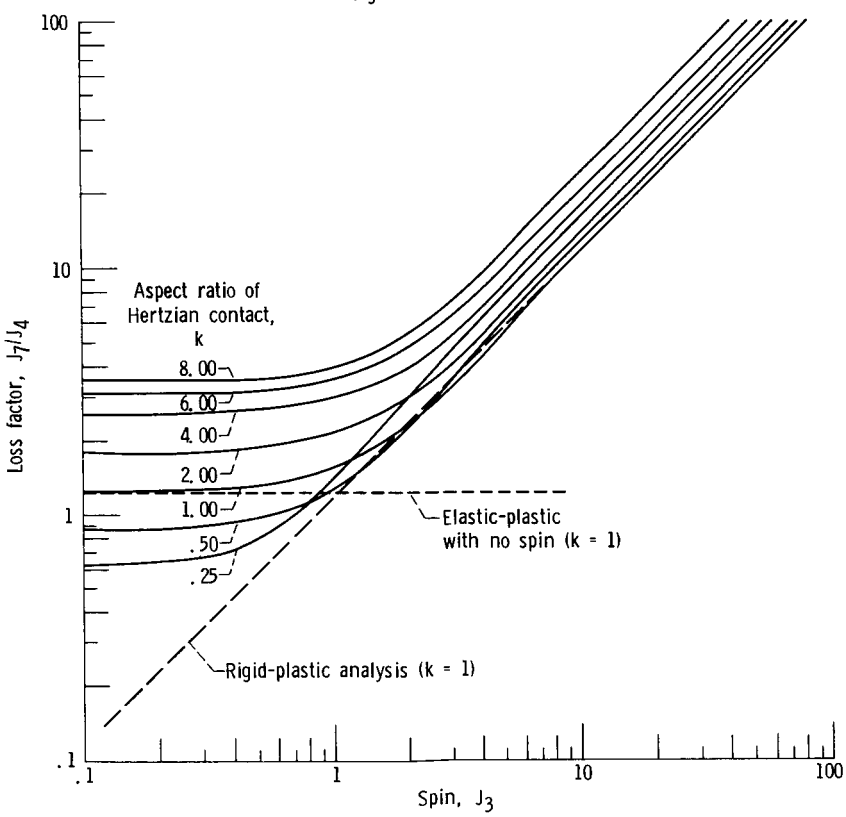

Figure 17. - Loss factor as a function of J_3 spin at various aspect ratios for J_4 = 0.75.

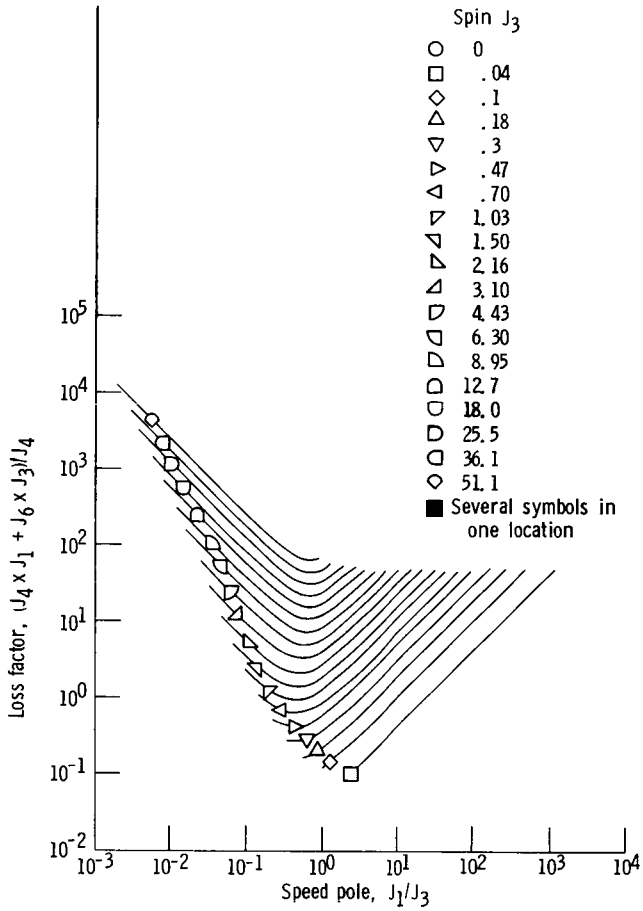

Figure 18. - Loss factor as function of ε speed pole location for at various values of spin J_3 for aspect ratio of Hertzian contact k = 1.00.

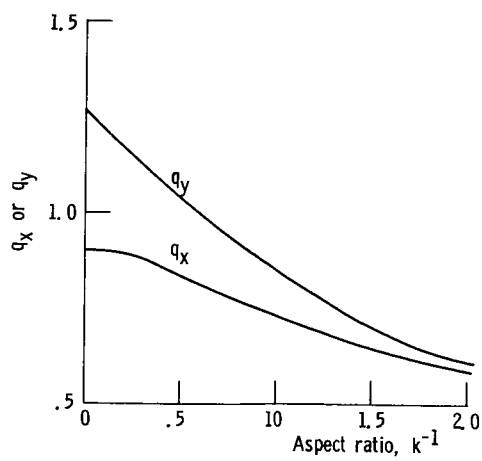

Figure 19. - Kalker coefficients q_x, q_y as function of aspect ratio k.

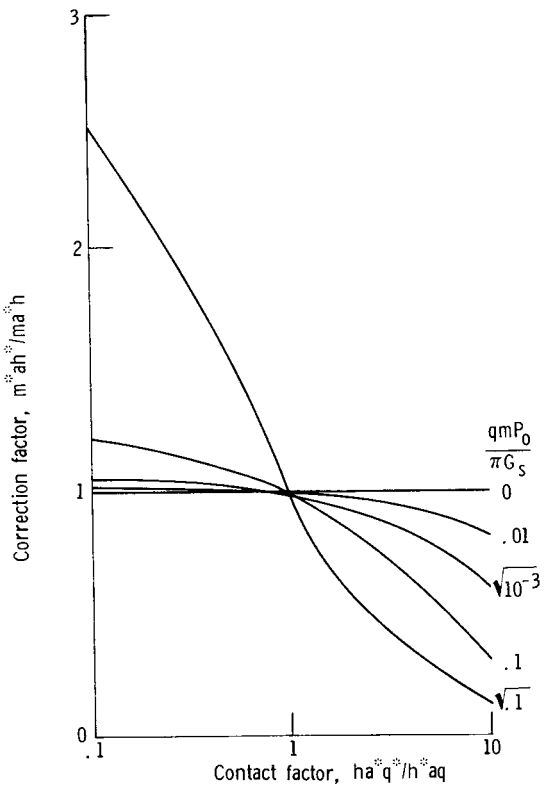

Figure 20. - Correction factors to convert slope m to m'.

1. Report No.	2. Government Accession No.	3. Recipient's Catalog No.
NASA TP-1530		

4. Title and Subtitle	5. Report Date
TRACTION DRIVE PERFORMANCE PREDICTION FOR THE JOHNSON AND TEVAARWERK TRACTION MODEL	October 1979
	6. Performing Organization Code
7. Author(s)	8. Performing Organization Report No.
Joseph L. Tevaarwerk	E-033
	10. Work Unit No.
9. Performing Organization Name and Address National Aeronautics and Space Administration Lewis Research Center Cleveland, Ohio 44135	11. Contract or Grant No.
	13. Type of Report and Period Covered Technical Paper
12. Sponsoring Agency Name and Address National Aeronautics and Space Administration Washington, D.C. 20546	14. Sponsoring Agency Code

15. Supplementary Notes

The author is at the University of Waterloo, Waterloo, Ontario, Canada; was a Summer Faculty Fellow at the Lewis Research Center in 1979.

16. Abstract

The recently developed Johnson and Tevaarwerk fluid rheology model is used to investigate the traction behavior for typical traction drive contacts. The influence of aspect ratio of the contact and the invariably present spin is investigated. Contacts with a low aspect ratio predict a superior performance in that they show less slip for the same degree of traction. Spin always has a diminishing effect on the traction at the same slip. At sufficiently high spin it is found that the Johnson and Tevaarwerk model may be further simplified to a limiting shear stress model. The conventional analysis by Wernitz applies here equally well.

17. Key Words (Suggested by Author(s))	18. Distribution Statement
Traction; Traction lubricant; Traction drives; Traction transmissions; Traction drive performance; Traction drive design	Unclassified - unlimited STAR Category 37

19. Security Classif. (of this report)	20. Security Classif. (of this page)	21. No. of Pages	22. Price*
Unclassified	Unclassified	40	A03

* For sale by the National Technical Information Service, Springfield, Virginia 22161

NASA-Langley, 1979